

# Phase diagrams in the three-flavor Nambu–Jona-Lasinio model with the Polyakov loop

Kenji Fukushima

*Yukawa Institute for Theoretical Physics, Kyoto University, Kyoto 606-8502, Japan*

We present extensive studies on hot and dense quark matter with two light and one heavy flavors in the Nambu–Jona-Lasinio model with the Polyakov loop (so-called PNJL model). First we discuss prescription dependence in choosing the Polyakov loop effective potential and propose a simple and rather sensible ansatz. We look over quantitative comparison to the lattice measurement to confirm that the model captures thermodynamic properties correctly. We then analyze the phase structure by changing the temperature, quark chemical potential, quark masses, and coupling constants. We particularly investigate how the effective  $U_A(1)$  restoration and the induced vector-channel interaction at finite density would affect the QCD critical point.

PACS numbers: 12.38.Aw, 11.10.Wx, 11.30.Rd, 12.38.Gc

## I. INTRODUCTION

The phase diagram of hot and dense matter out of quarks and gluons described by Quantum Chromodynamics (QCD) has attracted theoretical and experimental interest for decades [1, 2]. We can define one phase transition associated with chiral symmetry restoration in the vanishing quark mass limit (i.e.  $m_q \rightarrow 0$ ) which is commonly referred to as the chiral phase transition. In the quenched limit with infinitely heavy quark mass (i.e.  $m_q \rightarrow \infty$ ), on the other hand, we can define another phase transition from the hadron (glueball) phase to the color deconfinement phase. The question is then the nature of these phase transitions with intermediate quark masses of two light (*up* and *down*) and one heavy (*strange*) flavors. We stress that the chiral and deconfinement phase transitions are conceptually distinct phenomena and, theoretically speaking, they reside in the opposite limits with respect to the quark mass. Nevertheless, the standard QCD phase diagram on the plane of the temperature  $T$  and the chemical potential  $\mu$  has only a single transition or crossover boundary. Whether this is really the case is not trivial *a priori* and not quite settled yet.

It is the result from the Monte-Carlo integration of the (quenched) QCD partition function on the lattice that had led us to this phase diagram with a single phase boundary [3]. (See Ref. [4] and references therein for historical background.) Later on, the lattice QCD simulation with dynamical quarks [5] have confirmed that the chiral and deconfinement phase transitions occur at the same temperature (or at different but close temperatures [6]). This observation suggests that two phenomena of chiral restoration and color deconfinement should be locked by some dynamical mechanism so that they should take place (nearly) at once.

We can find the first successful study based on dynamical model to give an account for this locking mechanism in the work by Gocksch and Ogilvie [7]. They have constructed the effective action of QCD by means of the strong coupling and large dimensional expansions. The same action has been discussed at finite  $T$  and  $\mu$  also

by Ilgenfritz and Kripfgantz [8]. There were proposed some generic mixing arguments which aim to explain the coincidence of critical temperatures in a model independent way [9]. The mixing effect, however, does not suffice to force two crossovers to be a single one in view of the associated peaks in the susceptibility; two separate crossovers (susceptibility peaks) with mixing for each cannot be ruled out. That means, the mixing effect is a necessary but not sufficient condition in order to realize the coincidence in a way seen on the lattice [10]. Thus, the locking between chiral restoration and deconfinement should need more tangled dynamical properties of two phenomena.

To reveal the relevant dynamics, the present author proposed a useful model [13] based on the Nambu–Jona-Lasinio (NJL) model [11, 12] with the Polyakov loop degrees of freedom augmented, which was inspired by the strong coupling analyses [7, 8, 14]. The peculiar feature in this model is that we can uniquely determine the coupling between the chiral condensate, which is an order parameter for the chiral phase transition in  $m_q \rightarrow 0$ , and the Polyakov loop, which is an order parameter for the deconfinement phase transition in  $m_q \rightarrow \infty$ . The model inputs and outputs have been carefully compared to the lattice QCD data by Ratti, Thaler, and Weise [15] and they named this hybrid description as the *PNJL model*.

The PNJL model has been generalized to the three-flavor case recently [16, 17]. In the present paper we shall extensively explore the phase diagrams in the three-flavor PNJL model by changing four physical variables, namely,  $T$ ,  $\mu$ , the light quark mass  $m_{ud}$ , and the heavy quark mass  $m_s$ . First we revisit the choice of the Polyakov loop effective potential that cannot avoid ambiguity in the PNJL model approach. We claim that a careful consideration is necessary for the effective potential form. Once we fix the pure gluonic sector by specifying the potential, we can calculate the mean-fields of the chiral condensate and the Polyakov loop to draw the phase diagrams.

Although it is usually assumed implicitly, we have no first-principle insight into the locking of two crossovers in the finite-density region. The lattice Monte-Carlo simulation is of no practical use except when  $\mu$  is much smaller

than  $T$ . So far it seems that almost nothing but the PNJL model can access both transitions at any density. Strictly speaking, in fact, the mean-field treatment of the PNJL model is not totally free from the sign problem. Detailed analyses in Ref. [18] support that the saddle-point of the mean-field energy leads to an appropriate estimate for the mean-fields, however. Hence, we will not argue the sign problem any more in the present work.

In this paper, after we check that our results from the three-flavor PNJL model are consistent with the state-of-art lattice simulation at zero chemical potential [19], we will shift our emphasis toward the QCD (chiral) critical end-point in the last half. It should be noted that the terminal point of the first-order phase boundary has a second-order phase transition characterized by the universality class of the Z(2) Ising model and this special point is often called the QCD critical point. The search for the critical point is one of the most interesting problems in finite density QCD because it provides us with a firm milestone for our quest for the QCD phase diagram. If we are lucky enough to find out the critical point as predicted in theory, we can get confident about our theory reliability. This is, so to speak, a mutual correspondence between theory and experiment, which is an ideal situation for sound scientific developments.

The existence of the QCD critical point has not been established yet. We cannot exclude a possibility that the QCD phase transition is smooth everywhere in the  $\mu$ - $T$  plane, while there are a pile of indirect evidences for its existence [20, 21, 22, 23, 24, 25, 26]. In model studies, in fact, a minor modification in the treatment could easily smear a first-order phase transition out into a crossover, as demonstrated later. In particular we shall pay attention to two obscure factors which may significantly affect where the critical point is and even whether it exists. Those two factors are the magnitude of the  $U_A(1)$ -breaking anomaly interaction and the vector-channel interaction. The former, the  $U_A(1)$ -breaking term, induces a six-quark vertex called the 't Hooft term which mixes three different flavors up and is responsible for the first-order phase transition in the chiral limit [27]. It could be possible at finite temperature and density that the 't Hooft interaction is reduced by instanton suppression [28, 29, 30]. The latter effect, i.e. the vector-channel interaction term, does not break chiral symmetry and the zeroth component directly couples the quark density. It is thus likely that the finite-density environment enhances or induces interactions in the vector channel which could weaken the first-order phase transition [20, 31, 32, 33]. In this paper we shall quantify these effects on the location of the QCD critical point using the three-flavor PNJL model.

## II. MODEL SETUP

The present author proposed the PNJL model action in Ref. [13] inspired by the effective action in strong-

coupling QCD with dynamical quarks [7, 8, 14]. It is possible to some extent to elaborate a field-theoretical setup for the PNJL model starting with the Lagrangian density [15]. For this purpose it is required to assume a homogeneous mean-field distribution of the Polyakov loop. In other words, the temporal component of the gauge field,  $A_4$ , in Euclidean space-time must be approximated by a spatially constant mean-field, so that one can perform the one-loop integration with respect to thermal quarks in a closed form. This thermal integration leads to the unique coupling between the chiral condensate and the Polyakov loop. Spatial uniformity is in fact a mean-field ansatz, however, and it makes a contrast to the strong-coupling framework [14], as we shall discuss shortly.

In the PNJL model the Polyakov loop is therefore put in as a global mean-field rather than a local dynamical variable, which is analogous to the treatment of the chiral condensate in the ordinary NJL model; the Lagrangian density with a shift by the mean-field is sometimes referred to as the mean-field Lagrangian that contains no kinetic term for the mean-field. Such an approximation should work to investigate the bulk property of the thermodynamic system, while we have to be aware that the mean-field model cannot properly deal with the spatial structure of confined objects. It is beyond the scope of the simple PNJL model framework, for instance, to extract the heavy-quark potential.

All the model ingredients are thus given as mean-field variables. Here we would prefer to start with the mean-field free-energy after one-loop integration for the model setup. Let us decompose the free-energy below into four pieces and discuss them in order. That is, the total free-energy (or the grand potential) is a sum of four contributions;

$$\Omega_{\text{PNJL}} = \underbrace{\Omega_{\text{cond}} + \Omega_{\text{zero}} + \Omega_{\text{quark}}}_{\text{NJL part}} + \underbrace{\Omega_{\text{Polyakov}}}_{\text{pure gluonic part}}, \quad (1)$$

where  $\Omega_{\text{cond}}$  represents the condensation energy in the chiral sector,  $\Omega_{\text{zero}}$  the zero-point energy which is important in the NJL model formulation,  $\Omega_{\text{quark}}$  the thermal quark contribution with the Polyakov loop coupling coming from the Dirac determinant, and  $\Omega_{\text{Polyakov}}$  gives the effective potential in terms of the Polyakov loop variable. As indicated in Eq. (1), we can deduce the first three from the standard NJL model and the last one from the pure gluonic theory.

### A. Condensation Energy

We can read the condensation energy from the standard NJL model Lagrangian. Using the notation by Hatsuda and Kunihiro [12], we write the four-quark interaction in the scalar channel and the six-quark 't Hooft interaction as

$$\mathcal{L}_S = \frac{g_S}{2} [(\bar{\psi}\lambda_a\psi)^2 + (\bar{\psi}i\gamma_5\lambda_a\psi)^2], \quad (2)$$

and

$$\mathcal{L}_A = g_D [\det \bar{\psi} (1 - \gamma_5) \psi + \text{h.c.}] , \quad (3)$$

respectively. For later convenience we also give an expression for the vector-channel interaction;

$$\mathcal{L}_V = -g_V (\bar{\psi} \gamma_\mu \psi)^2 . \quad (4)$$

For the moment we will work only in the  $g_V = 0$  case. Here,  $\lambda_a$ 's are the Gell-Mann matrices in flavor space (with  $\lambda_0 = \sqrt{2/3}$ ) and the matrix determinant is taken also in flavor space. In the mean-field approximation with three condensates,  $\langle \bar{u}u \rangle$ ,  $\langle \bar{d}d \rangle$ , and  $\langle \bar{s}s \rangle$ , the scalar four-quark interaction is rewritten as

$$\begin{aligned} g_S (\bar{u}u)^2 &\rightarrow g_S (\bar{u}u - \langle \bar{u}u \rangle + \langle \bar{u}u \rangle) (\bar{u}u - \langle \bar{u}u \rangle + \langle \bar{u}u \rangle) \\ &\simeq g_S \langle \bar{u}u \rangle^2 + 2g_S \langle \bar{u}u \rangle (\bar{u}u - \langle \bar{u}u \rangle) \\ &= -g_S \langle \bar{u}u \rangle^2 + 2g_S \langle \bar{u}u \rangle \bar{u}u , \end{aligned} \quad (5)$$

in the  $u$ -quark sector and likewise for  $d$ -quarks and  $s$ -quarks. In this way we can readily reach the following expression for the condensation energy;

$$\Omega_{\text{cond}} = g_S (\langle \bar{u}u \rangle^2 + \langle \bar{d}d \rangle^2 + \langle \bar{s}s \rangle^2) + 4g_D \langle \bar{u}u \rangle \langle \bar{d}d \rangle \langle \bar{s}s \rangle . \quad (6)$$

We see that the six-quark interaction induces the flavor-mixing interaction indeed which makes the phase transition of first-order in the presence of massless three flavors.

### B. Zero-Point Energy

The zero-point energy diverges and requires the ultraviolet cutoff  $\Lambda$  to regularize the three-momentum integration. Since the NJL model is a non-renormalizable cutoff theory depending on the choice of  $\Lambda$ , the zero-point energy contribution largely affects the model output. With the quasi-quark energy dispersion relation,  $\varepsilon_i(p) = \sqrt{p^2 + M_i^2}$ , the zero-point energy can be expressed simply as a summation of all  $\varepsilon_i(p)/2$ , that is,

$$\Omega_{\text{zero}} = -2N_c \sum_i \int^\Lambda \frac{d^3p}{(2\pi)^3} \varepsilon_i(p) , \quad (7)$$

where 2 is the spin degrees of freedom,  $N_c = 3$  is the number of colors, and the particle and anti-particle contributions cancel 2 in the denominator of  $\varepsilon_i(p)/2$ . The constituent quark mass is defined as a sum of the current quark mass and the mean-field as

$$\begin{aligned} M_u &= m_u - 2g_S \langle \bar{u}u \rangle - 2g_D \langle \bar{d}d \rangle \langle \bar{s}s \rangle , \\ M_d &= m_d - 2g_S \langle \bar{d}d \rangle - 2g_D \langle \bar{s}s \rangle \langle \bar{u}u \rangle , \\ M_s &= m_s - 2g_S \langle \bar{s}s \rangle - 2g_D \langle \bar{u}u \rangle \langle \bar{d}d \rangle , \end{aligned} \quad (8)$$

which is understood from the second term in Eq. (5).

### C. Thermal Quark Energy

The thermal quark energy is where we can uniquely introduce coupling between the chiral condensate and the Polyakov loop. In the PNJL model, under the assumption of the presence of the spatially uniform Polyakov loop background, the one-loop free-energy is modified as

$$\begin{aligned} \Omega_{\text{quark}} &= -2T \sum_i \int \frac{d^3p}{(2\pi)^3} \left\{ \ln \det \left[ 1 + L e^{-(\varepsilon_i(p) - \mu)/T} \right] \right. \\ &\quad \left. + \ln \det \left[ 1 + L^\dagger e^{-(\varepsilon_i(p) + \mu)/T} \right] \right\} . \end{aligned} \quad (9)$$

Let us comment on preceding works [34, 35] in which a similar coupling form is addressed.

We note that the above expression is identical with that in the strong coupling expansion but the physics content is slightly different. The Polyakov loop  $L$  is a mean-field from the beginning here, whereas the strong coupling calculation at finite temperature decouples the temporal hopping from spatial link variables [14]. As a result, the quark excitation is static in the strong-coupling leading order, and the above expression results at each lattice site in this way, that is,  $L$  could be a local variable in the strong coupling expansion.

It is noteworthy that the three-momentum integration above is finite and has no need for the ultraviolet cutoff. We can thus relax the cutoff in the thermal quark energy, though we found that the  $s$ -quark sector behaves unnaturally at extremely high temperature without the cutoff, which is of no importance practically. In this work we will not impose the momentum cutoff onto the thermal quark energy in order to let the thermodynamic quantities free from cutoff artifact.

The Polyakov loop  $L$  is an  $N_c \times N_c$  matrix in color space and is defined originally in terms of  $A_4$ . The explicit form of the Polyakov loop is irrelevant in our study because we treat it as a model variable and will not return to the original definition of the Polyakov loop in terms of the gauge field.

In the simplest mean-field approximation one can express the free-energy as a function of the traced Polyakov loop expectation value defined by

$$\ell = \frac{1}{N_c} \langle \text{tr} L \rangle , \quad \bar{\ell} = \frac{1}{N_c} \langle \text{tr} L^\dagger \rangle . \quad (10)$$

It should be mentioned that we must distinguish  $\ell$  and  $\bar{\ell}$  at finite density [18, 36, 37]; both  $\ell$  and  $\bar{\ell}$  are real, and nevertheless,  $\bar{\ell} > \ell$  whenever  $\mu > 0$ . This is because a finite chemical potential gives rise to a  $C$ -odd term like  $\mu \text{Im}[\text{tr} L]$  in the average weight leading to  $\bar{\ell} - \ell \sim \mu \langle (\text{Im}[\text{tr} L])^2 \rangle > 0$  for small  $\mu$ . We can also give an intuitive explanation;  $\bar{\ell}$  represents the exponential of the free-energy gain,  $f_{\bar{\ell}}$ , by the presence of an anti-quark. The test charge brought in by an anti-quark can be more easily screened in a medium with more quarks than anti-quarks. Therefore,  $f_{\bar{\ell}} < f_{\ell}$ , that means,  $\bar{\ell} = e^{-f_{\bar{\ell}}/T} > \ell = e^{-f_{\ell}/T}$  for a positive  $\mu$ .

It is straightforward to take an average of the  $3 \times 3$  determinant to reach

$$\begin{aligned} \left\langle \det[1 + L e^{-(\varepsilon-\mu)/T}] \right\rangle &= 1 + e^{-3(\varepsilon-\mu)/T} \\ &+ 3 \ell e^{-(\varepsilon-\mu)/T} + 3 \bar{\ell} e^{-2(\varepsilon-\mu)/T}, \end{aligned} \quad (11)$$

$$\begin{aligned} \left\langle \det[1 + L^\dagger e^{-(\varepsilon+\mu)/T}] \right\rangle &= 1 + e^{-3(\varepsilon+\mu)/T} \\ &+ 3 \bar{\ell} e^{-(\varepsilon+\mu)/T} + 3 \ell e^{-2(\varepsilon+\mu)/T}. \end{aligned} \quad (12)$$

In this work we use the logarithm of the above expressions as the mean-field free-energy and will not perform the group integration over  $L$ . Roughly speaking, the approximation involving the group integration [7] corresponds to what is called the Weiss mean-field approximation in the spin system. The integration has an effect on the quantitative results [38] but a simple mean-field treatment suffices for our present purpose. We also remark that the action is invariant under simultaneous replacement  $\ell \leftrightarrow \bar{\ell}$  and  $-\mu \leftrightarrow +\mu$ .

#### D. Polyakov Loop Energy

In the definition of the PNJL model the choice of the Polyakov loop potential has subtlety because the effective potential has not been known directly from the lattice QCD simulation. In the present study we will assume the strong-coupling inspired form of

$$\begin{aligned} \Omega_{\text{Polyakov}} &= -b \cdot T \left\{ 54 e^{-a/T} \ell \bar{\ell} \right. \\ &\left. + \ln[1 - 6 \ell \bar{\ell} - 3(\ell \bar{\ell})^2 + 4(\ell^3 + \bar{\ell}^3)] \right\}. \end{aligned} \quad (13)$$

The logarithmic term appears from the Haar measure of the group integration with respect to the SU(3) Polyakov loop matrix. The first term is reminiscent of the nearest neighbor interaction in the effective action at strong coupling. The temperature-dependent coefficient of this  $\ell \bar{\ell}$  term controls the deconfinement phase transition temperature.

In this simple ansatz for the Polyakov loop potential, we have two parameters;  $a$  and  $b$ . The deconfinement phase transition is determined solely by the choice of  $a$ , while  $b$  parametrizes the relative strength of mixing between the chiral and deconfinement phase transitions. If  $b$  is small, chiral restoration dominates the phase transition, and if  $b$  is large, deconfinement is more governing.

We will numerically make a comparison between the above-proposed ansatz and others in the next section.

### III. NUMERICAL PROCEDURES

Now that we have specified all the constituents in the model action, we get ready to proceed to the numerical analyses. We will solve the following four equations in a

self-consistent way,

$$\frac{\partial \Omega_{\text{PNJL}}}{\partial \langle \bar{u}u \rangle} = \frac{\partial \Omega_{\text{PNJL}}}{\partial \langle \bar{s}s \rangle} = \frac{\partial \Omega_{\text{PNJL}}}{\partial \ell} = \frac{\partial \Omega_{\text{PNJL}}}{\partial \bar{\ell}} = 0 \quad (14)$$

to acquire  $\langle \bar{u}u \rangle = \langle \bar{d}d \rangle$ ,  $\langle \bar{s}s \rangle$ ,  $\ell$ , and  $\bar{\ell}$  as functions of the model input. For this purpose we have to fix all the model parameters,  $\Lambda$ ,  $g_S$ ,  $g_D$  in the NJL potential, and  $a$  and  $b$  in the Polyakov loop potential.

#### A. Parameter Choice

The Polyakov loop coupling appears only in the thermal part, that means that the NJL model parameters fixed at  $T = \mu = 0$  are not affected by introduction of the Polyakov loop coupling. In this work we will employ the widely accepted parameter set according to Hatsuda and Kunihiro [12];

$$\begin{aligned} \Lambda &= 631.4 \text{ MeV}, \\ m_{ud} &= 5.5 \text{ MeV}, \quad m_s = 135.7 \text{ MeV}, \\ g_S \cdot \Lambda^2 &= 3.67, \quad g_D \cdot \Lambda^5 = -9.29, \end{aligned} \quad (15)$$

which nicely reproduces the  $\pi$  mass, the  $K$  mass, the  $\eta'$  mass, and the  $\pi$  decay constant  $f_\pi$ . Here  $m_{ud}$  stands representatively for the light quark mass, i.e.  $m_{ud} = m_u = m_d$ .

Regarding the Polyakov loop potential, we can fix the parameter  $a$  by the condition that the first-order phase transition in the pure gluodynamics takes place at  $T = 270 \text{ MeV}$ , which yields

$$a = 664 \text{ MeV}, \quad (16)$$

and then the remaining variable is  $b$  only. Actually, the determination of  $b$  suffers uncertainty and there is no established prescription. In this study we shall take a value of  $b$  that leads to simultaneous crossovers of chiral restoration and deconfinement around  $T \simeq 200 \text{ MeV}$ . As a result, we set

$$b \cdot \Lambda^{-3} = 0.03. \quad (17)$$

#### B. Other Polyakov Loop Potentials

The choice of the Polyakov loop potential has some variations, as we have mentioned before. Our choice of Eq. (13) is much simpler than the widely accepted forms by Ratti, Thaler, and Weise [15] and by Rößner, Ratti, and Weise [39]. It would be instructive to scrutinize respective forms and quantify the difference numerically. Let us call the “RTW05 potential” to indicate

$$\Omega_{\text{RTW05}} = T^4 \left[ -\frac{b_2(T)}{2} \ell \bar{\ell} - \frac{b_3}{6} (\ell^3 + \bar{\ell}^3) + \frac{b_4}{4} (\ell \bar{\ell})^2 \right] \quad (18)$$

with  $b_2(T) = a_0 + a_1(T_0/T) + a_2(T_0/T)^2 + a_3(T_0/T)^3$ , which is proposed in Ref. [15]. There are seven parameters,  $a_0 = 6.76$ ,  $a_1 = -1.95$ ,  $a_2 = 2.625$ ,  $a_3 = -7.44$ ,

$b_3 = 0.75$ ,  $b_4 = 7.5$ , and  $T_0 = 270$  MeV such that the potential (18) reproduces the pressure, energy density, and entropy density in the pure gluonic sector measured on the lattice. A slightly different choice is suggested in Ref. [39] which we shall call the “RRW06 potential”;

$$\Omega_{\text{RRW06}} = T^4 \left\{ -\frac{a(T)}{2} \ell \bar{\ell} + b(T) \ln[1 - 6\ell \bar{\ell} - 3(\ell \bar{\ell})^2 + 4(\ell^3 + \bar{\ell}^3)] \right\} \quad (19)$$

with  $a(T) = a_0 + a_1(T_0/T) + a_2(T_0/T)^2$  and  $b(T) = b_3(T_0/T)^3$ . Five parameters are fixed as  $a_0 = 3.51$ ,  $a_1 = -2.47$ ,  $a_2 = 15.2$ ,  $b_3 = -1.75$ , and  $T_0 = 270$  MeV. We note that  $b_3$  plays the same role as  $b$  in our ansatz (13). Actually, if we substitute  $T_0 = 190$  MeV to lower the crossover temperature as argued in Ref. [15],  $b_3 T_0^3 \cdot \Lambda^3 \simeq 0.044$  (where  $\Lambda$  is not our value but 650 MeV used in Ref. [15]) which turns out to be comparable to our choice (17).

Under the assumption that  $\Omega_{\text{RTW05}}$  and  $\Omega_{\text{RRW06}}$  correspond to the *total* negative pressure in the pure gluonic theory, they approach the Stefan-Boltzmann limit at high temperature, that is,  $p = (2 \cdot 8 \cdot \pi^2/90)T^4 = 1.75T^4$ . One can easily make this sure from  $-a_0/2 - b_3/3 + b_4/4 = -1.75$  in  $\Omega_{\text{RTW05}}$  and  $-a_0/2 = -1.75$  in  $\Omega_{\text{RRW06}}$ .

We would claim, however, that  $\Omega_{\text{RTW05}}$  and  $\Omega_{\text{RRW06}}$  might overcount the relevant degrees of freedom in the system. In the high temperature limit not only the Polyakov loop but also the deconfined transverse gluons contribute to the pressure. Since the Polyakov loop corresponds to the longitudinal gauge field, the Stefan-Boltzmann limit should be saturated by the transverse gluons but not the Polyakov loop. It is thus a subtle assumption that the effective potential with respect to the order parameter field can reproduce the total pressure, energy density, and entropy density for all temperatures.

One can understand this from a more familiar example. Let us consider the mean-field effective potential in the O(4) linear sigma model. The effective potential with respect to the  $\sigma$  condensate describes the chiral phase transition. The total pressure should contain contributions from the  $\pi$  excitations too which are not fully included in the effective potential in terms of  $\langle \sigma \rangle$ .

It is not our point to insist that  $\Omega_{\text{RTW05}}$  and  $\Omega_{\text{RRW06}}$  are doubtful. Our main point lies in the other way around in fact. We presume that their parametrization works in effect for the following reason; the pressure contribution from transverse gluons is a function of  $T$ , and the Polyakov loop is also a function of  $T$ , and so the former can be implicitly parametrized by the latter. Then, it is possible to express the total pressure in the form of Eq. (18) or (19). One has to keep in mind, however, that the total pressure in this interpretation would make sense provided that the Polyakov loop is already solved as a function of  $T$ . Therefore, one should solve Eq. (14) first and then one can fit the total pressure using Eq. (18) or (19) with solved  $\ell(T)$  and  $\bar{\ell}(T)$  substituted. One should

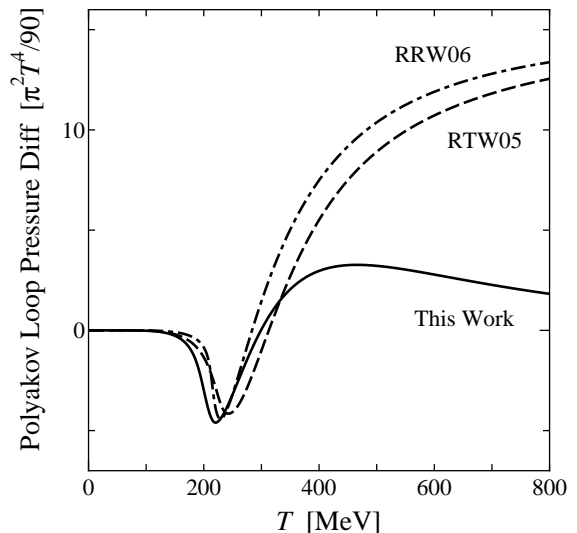


FIG. 1: Comparison of the Polyakov loop pressure excess as a function of the temperature. The vertical axis signifies the effective degrees of freedom. RTW05 and RRW06 represent  $\Omega_{\text{RTW05}}$  and  $\Omega_{\text{RRW06}}$  with  $\ell$  and  $\bar{\ell}$  given as a solution of the *full* gap equation with two quark flavors. For comparison we used the same NJL model parameters,  $\Lambda$ ,  $g_s$ , and  $m_u = m_d$  as in Ref. [15] and quenched the  $s$ -quark sector to draw the solid curve which represents our  $\Omega_{\text{Polyakov}}$ .

not use the total pressure itself to optimize the variational parameters  $\ell$  and  $\bar{\ell}$ . This may explain why the critical temperature determined with Eq. (18) or (19) put into the gap equations becomes relatively higher. The Polyakov loop effective potential which overcounts the gluonic degrees of freedom would drag the crossover point closer to the pure gluonic transition temperature  $T_0 = 270$  MeV.

We emphasize that our simple choice of the Polyakov loop potential is physically natural and, interestingly, it makes only little difference from the numerical results based on the RTW05 or RRW06 potential. This sounds very good, for our new potential ansatz does not ruin the nice agreement to the lattice data addressed in Refs. [15, 39, 40]. In Fig. 1 we plot the Polyakov loop pressure difference from the zero temperature value using the mean-fields obtained from the full gap equations with two flavors. In the absence of interaction, the pressure is given by the Stefan-Boltzmann law,  $\pi^2 T^4/90$ , multiplied by the effective degrees of freedom which we denote by  $\nu$ . To see how  $\nu$  increases as  $T$  goes up, we normalize the pressure by the Stefan-Boltzmann unit;  $\pi^2 T^4/90$ . Clearly both  $\Omega_{\text{RTW05}}$  and  $\Omega_{\text{RRW06}}$  increase with increasing  $T$  and asymptotically approach the value of  $\nu = 2$  (polarization)  $\times 8$  (color) = 16. It is so by construction, as we explained. It is intriguing to note that our ansatz (13) results in the solid curve in Fig. 1 which is close to the dashed and dot-dashed curves by  $\Omega_{\text{RTW05}}$  and  $\Omega_{\text{RRW06}}$  as long as the temperature is below  $300 \text{ MeV} \simeq 1.5T_c$ . We do not have to care much about the discrepancy in

the higher temperature region, in fact, because the validity region in the present study extends at best up to  $\sim 2T_c$  above which transverse gluons should be dominant. Therefore, we can conclude that all these potential choices are consistent to each other within the validity range of the temperature. In our choice (13) the effective degrees of freedom slowly decrease at higher temperature in the Stefan-Boltzmann unit. This is reasonable because the Polyakov loop must give way to transverse gluons.

The nearly coincidence of three curves in the vicinity of  $T_c$  in Fig. 1 delivers us an important message. The Polyakov loop takes on a major fraction of the system pressure up to the temperature around  $1.5T_c$ . We should recall that two parameters,  $a$  and  $b$ , in Eq. (13) have been fixed not to reproduce the pressure but just to yield  $T_0 = 270$  MeV in the pure gluonic sector and  $T_c \simeq 200$  MeV with  $2 + 1$  flavors.

#### IV. ZERO DENSITY RESULTS

Here we show the model results at zero quark density with our choice of the model parameters. In our subsequent discussions we will make clear the virtues of the PNJL model as well as some caveats.

##### A. Order Parameters

Because nothing breaks isospin symmetry in this work, we will show the numerical results only for the  $u$ -quark sector which is degenerate to the  $d$ -quark sector.

First of all, we present Fig. 2 to confirm that simultaneous crossovers of deconfinement and chiral restoration certainly realize in the PNJL model. The chiral condensates are normalized by their zero-temperature value;  $\langle \bar{u}u \rangle_0 = (246 \text{ MeV})^3$  and  $\langle \bar{s}s \rangle_0 = (267 \text{ MeV})^3$  for light and heavy quarks, respectively.

The reason why we find the simultaneous crossovers around  $T_c \simeq 200$  MeV (the temperature derivative gives  $T_c = 204.8$  MeV) is that we have chosen the value of  $b$  as Eq. (17) to adjust the crossover temperature by hand. Thus, we note that the crossover temperature is not the model output but the input. Nevertheless we would comment on a non-trivial feature inherent in the model dynamics; the chiral phase transition can never occur until the Polyakov loop grows up [13]. It is also interesting to look at the behavior of the  $s$ -quark chiral condensate depicted by the dotted curve. The results for  $\langle \bar{s}s \rangle$  are the output rather than the input unlike  $\langle \bar{u}u \rangle$ . If we define a crossover temperature for the  $s$ -quark sector, it should be higher than the simultaneous crossovers due to the explicit breaking of chiral symmetry.

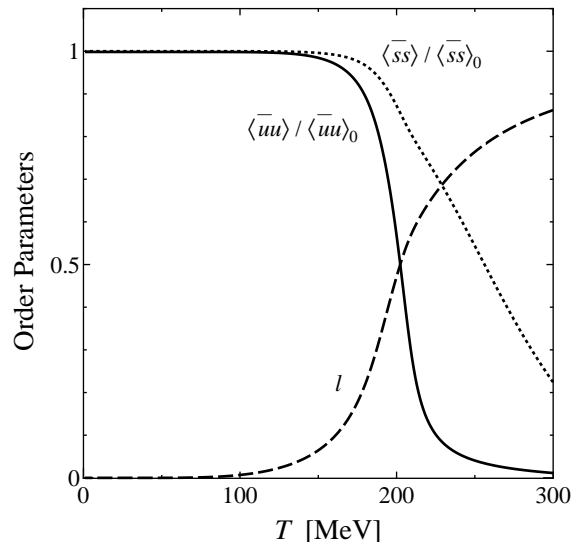


FIG. 2: Order parameters at zero density as a function of the temperature. The chiral condensates are normalized by  $\langle \bar{u}u \rangle_0 = (246 \text{ MeV})^3$  and  $\langle \bar{s}s \rangle_0 = (267 \text{ MeV})^3$ . The solid and dotted curves represent the  $u$ -quark and  $s$ -quark chiral condensates, respectively, and the dashed curve represents the traced Polyakov loop  $\ell$ .

##### B. Effective Confinement

Let us elucidate how the *effective* confinement is possible in the model description. The underlying idea in the PNJL model is that the group integration (average) with respect to the Polyakov loop acts as a projection onto the center symmetric state (or the *canonical ensemble* [41] with zero  $Z_3$  charge) if there is no Polyakov loop mean-field. We solve the four coupled equations (14) at  $T \neq 0$  and  $\mu = 0$ , and plot the quark pressure difference from the zero temperature value in Fig. 3 using the obtained mean-fields.

In the limit of massless two and three flavors we can count the fermionic degrees of freedom as  $\nu = (7/8) \cdot 3 \cdot 2 \cdot 4 = 21$  and  $\nu = (7/8) \cdot 3 \cdot 3 \cdot 4 = 31.5$ , respectively. Because the system of our interest is quark matter with two light and one heavy flavors,  $\nu$  should take a certain value between 21 and 31.5 at temperature above  $T_c$  where chiral symmetry is restored. This expectation is manifest in view of Fig. 3 both in the NJL model and in the PNJL model. Here we have determined the pseudo-critical temperature by the location where the temperature derivative,  $\partial \langle \bar{u}u \rangle / \partial T$ , is largest. It follows that  $T_c = 171.6$  MeV for the NJL model results and  $T_c = 204.8$  MeV for the PNJL model results (see also Fig. 2).

Even in the standard NJL model the effective degrees of freedom go down as the temperature becomes lower. This is because quark excitations are suppressed by the constituent quark mass in the low temperature side where chiral symmetry is spontaneously broken. In reality the

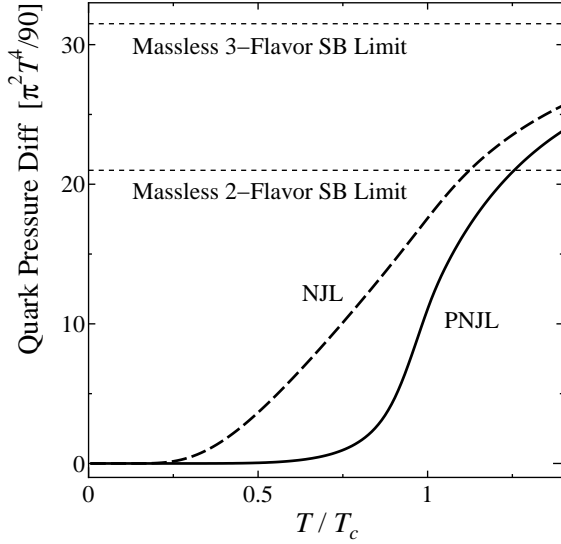


FIG. 3: Effective degrees of freedom associated with 2 + 1 flavor quarks with increasing temperature in the NJL model and in the PNJL model. The critical temperature is  $T_c = 171.6$  MeV in the NJL model case and  $T_c = 204.8$  MeV in the PNJL model case.

system should be mainly composed of a gas of  $\pi^0$  and  $\pi^\pm$  below  $T_c$  but the  $\pi$  mass is  $\sim 135$  MeV which is comparable to the critical temperature. It is thus expected that we can neglect the  $\pi$  loop corrections in the pressure in the first approximation.

We can see from Fig. 3 that the NJL model contains too many (unphysical) quark excitations below  $T_c$ . These fictitious excitations diminish only slowly. It is apparent that the Polyakov loop projection works efficiently in the PNJL model case. The effective degrees of freedom rapidly decrease near  $T_c$ , that means that artificial quark excitations are removed by the Polyakov loop coupling. Therefore, we can anticipate that the PNJL model should be more capable to capture realistic thermodynamics than the standard NJL model especially at temperatures near  $T_c$ . Also, because the Polyakov loop projection affects the quark sector, it is a natural expectation that the PNJL model would be a more suitable description than the NJL model in the finite density region where quarks exist abundantly.

Finally we shall remark that the separation of the total pressure into the Polyakov loop and the quark contributions like in Figs. 1 and 3 does not make sense in the mean-field approximation. This is because each of  $\langle \bar{u}u \rangle$ ,  $\langle \bar{s}s \rangle$ ,  $\ell$ , and  $\bar{\ell}$  determined by the gap equations (14) involve entangled contributions and thus a clear separation is impossible in any way.

### C. Susceptibility

In this subsection we clarify how we can evaluate the susceptibility in respective channels of our interest. A

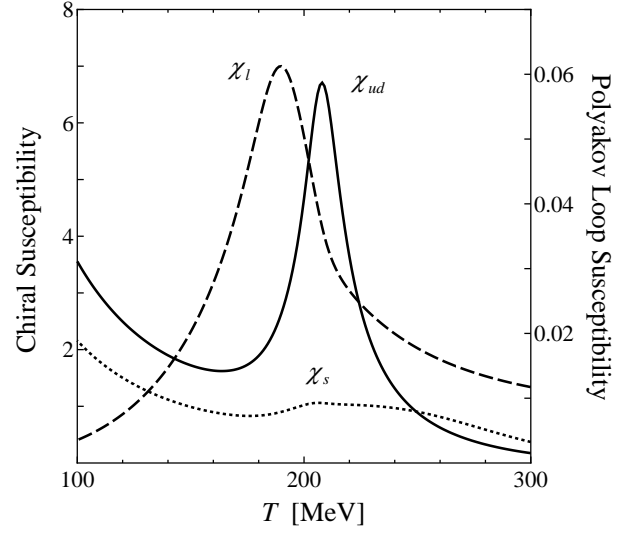


FIG. 4: Chiral and Polyakov loop susceptibility at zero density as a function of the temperature in the 2 + 1 flavor PNJL model.

useful alternative is to be deduced from the temperature slope, i.e.  $-\partial\langle\bar{u}u\rangle/\partial T$ ,  $\partial\ell/\partial T$ , and so on. They behave as a function of  $T$  in a similar manner as the susceptibility but the temperature slope is not really informative more than the order parameter curves read from Fig. 2.

In order to compute the susceptibility in the mean-field model we need some caution. Remembering that the logarithm of the partition function is  $-V\Omega_{\text{PNJL}}/T$ , we can give the definition of the dimensionless susceptibility of our interest as

$$\chi_{ud} = \frac{1}{4T} \frac{\partial^2(-\Omega_{\text{PNJL}}/T)}{\partial m_{ud}^2}, \quad (20)$$

$$\chi_s = \frac{1}{T} \frac{\partial^2(-\Omega_{\text{PNJL}}/T)}{\partial m_s^2}, \quad (21)$$

$$\chi_\ell = T^3 \frac{\partial^2(-\Omega_{\text{PNJL}}/T)}{\partial \eta \partial \bar{\eta}}, \quad (22)$$

$$\chi_q = \frac{1}{T} \frac{\partial^2(-\Omega_{\text{PNJL}}/T)}{\partial \mu^2}, \quad (23)$$

for the light-quark susceptibility, the heavy-quark susceptibility, and the Polyakov loop susceptibility, respectively. We also enumerate the quark number susceptibility that we will discuss later. Here we have inserted the Polyakov loop source  $\eta$  and  $\bar{\eta}$  in the potential as  $\Omega_{\text{Polyakov}} \rightarrow \Omega_{\text{Polyakov}} - T(\eta\ell + \bar{\eta}\bar{\ell})$ . It is crucial to notice that we have to take the derivative in a way that it hits the mean-fields also. That means that we should take  $\partial\langle\bar{u}u\rangle/\partial m_{ud}$ ,  $\partial^2\langle\bar{u}u\rangle/\partial m_{ud}^2$ ,  $\partial\langle\bar{s}s\rangle/\partial m_{ud}$ ,  $\partial^2\langle\bar{s}s\rangle/\partial m_{ud}^2$ ,  $\partial\ell/\partial m_{ud}$ ,  $\partial^2\ell/\partial m_{ud}^2$ , etc into account to evaluate Eq. (20) for instance. Otherwise we would miss the loop effect and the mixing to other channels.

We can justify this procedure by evaluating the susceptibility in an independent (and equivalent) method.

By definition, in general, the susceptibility is to be identified as the inverse of the potential curvature. For the purpose to compute the curvature inverse, we should consider the curvature matrix  $C$  whose dimensionless components are given by  $C_{uu} = T^2 \partial^2 \Omega_{\text{PNJL}} / \partial \langle \bar{u}u \rangle^2$ ,  $C_{us} = T^2 \partial^2 \Omega_{\text{PNJL}} / \partial \langle \bar{u}u \rangle \partial \langle \bar{s}s \rangle$ ,  $C_{u\ell} = T^{-1} \partial^2 \Omega_{\text{PNJL}} / \partial \langle \bar{u}u \rangle \partial \ell$ ,  $C_{\ell\ell} = T^{-4} \partial^2 \Omega_{\text{PNJL}} / \partial \ell \partial \bar{\ell}$ , and so on. In the present case  $C$  is a  $4 \times 4$  matrix. Then the diagonal components of  $C^{-1}$  give the susceptibility which is an involved expression in terms of  $C_{uu}$ ,  $C_{us}$ ,  $C_{u\ell}$ , etc. Roughly speaking, the diagonal part,  $C_{uu}^{-1}$ ,  $C_{ss}^{-1}$ ,  $C_{\ell\ell}^{-1}$ , corresponds to soft-mode propagators and the off-diagonal part,  $C_{us}$ ,  $C_{u\ell}$ ,  $C_{\ell\ell}$ ,  $C_{\ell\bar{\ell}}$ , and so on, corresponds to mixing vertices. It is immediate to make sure that  $C^{-1}$  certainly leads to exactly the same results as obtained from Eqs. (20), (21), and (22). This matrix method has an advantage in giving us the mixing angle between each mode.

As we can notice from Fig. 4 showing the susceptibility as a function of  $T$ , two crossovers associated with  $\langle \bar{u}u \rangle$  and  $\ell$  are located close to each other but do not coincide precisely. As long as we treat the chiral condensate and the Polyakov loop as independent variables as in the PNJL model, two crossovers attract each other to some extent but have a short “repulsion.” Within this kind of model approach it is hence hard to explain the complete coincidence without fine tuning.

One interesting strategy is not to explain the locking but to build a new model based on the complete locking of chiral restoration and deconfinement. As discussed in Ref. [10], most of lattice results support the idea that there is only one order parameter field  $\phi$  that is a mixture of the  $\sigma$  meson and the electric glueball (Polyakov loop). Then, we could make a model with the chiral condensate given by  $\langle \bar{u}u \rangle \propto \phi \cos \theta$  and the Polyakov loop by  $\ell \propto \phi \sin \theta$  with some potential energy for the mixing angle  $\theta$  between them. The work along this direction is under progress [42].

#### D. Quark Number Susceptibility

It is difficult to probe physical observables sensitive to the chiral and Polyakov loop susceptibility directly in experiments. In fact, it is impossible to count the number fluctuation of the  $\sigma$  meson and the glueball which eventually decay to the lightest  $\pi$  meson. From the experimental point of view the quark number susceptibility should be a better measure because the quark number is a conserved quantity. The fluctuation in the baryon multiplicity would be directly related to the quark number susceptibility,  $\chi_q$  [12, 24, 43]. Also in Refs. [40, 44]  $\chi_q$  has been evaluated and discussed in the two-flavor PNJL model. Actually the PNJL model can reproduce  $\chi_q$  measured on the lattice in the two-flavor case as beautifully illustrated in Ref. [40].

We plot our results in the  $2 + 1$  flavor case in Fig. 5. We can see, as expected, that the  $2 + 1$  flavor quark matter yields  $\chi_q$  greater than the two-flavor case shown

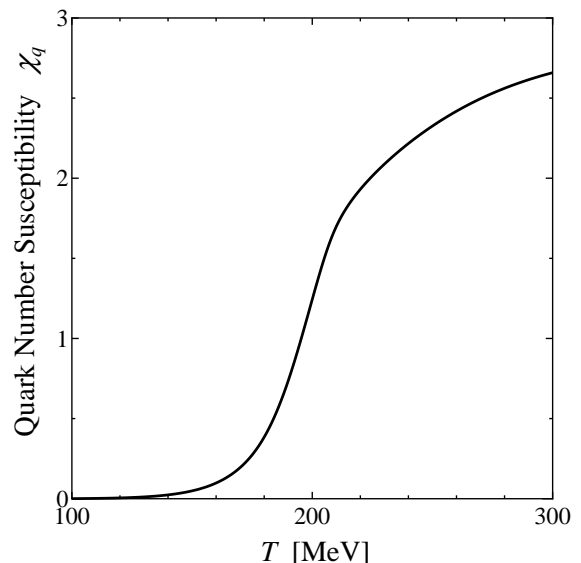


FIG. 5: Quark number susceptibility calculated in the PNJL model for  $2 + 1$  flavor quark matter at zero density.

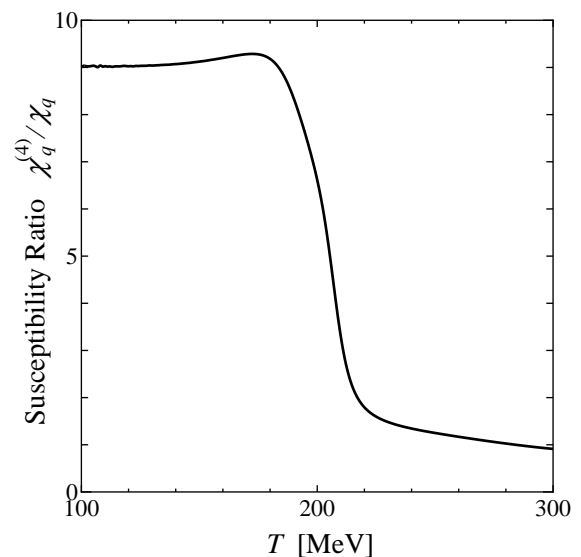


FIG. 6: Ratio of the fourth derivative to the quark number susceptibility calculated in the PNJL model for  $2 + 1$  flavor quark matter at zero density.

in Ref. [40]. In the chiral limit  $\chi_q$  would scale as  $N_f^2$ , and thus the three-flavor value should be  $3^2/2^2 = 2.25$  times greater than the two-flavor value. Because  $s$ -quarks are massive in reality, this scale factor should become smaller. Let us choose one temperature to take an example for comparison. At the temperature  $T = 1.5T_c \simeq 300$  MeV, Fig. 5 reads around 2.7, while the two-flavor value is around 1.5, which leads to the ratio 1.8. This seems to be a reasonable number.



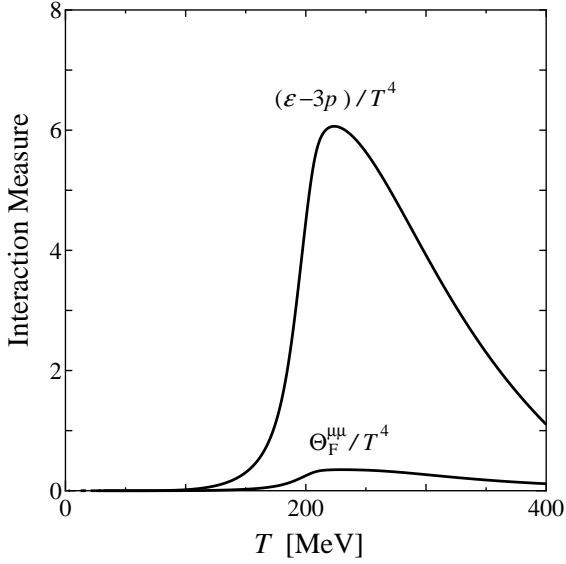


FIG. 7: Plot for the “interaction measure,” i.e.  $(\epsilon - 3p)/T^4$ , and the fermion contribution,  $\Theta_F^{\mu\mu} = [2m_{ud}(\langle \bar{u}u \rangle - \langle \bar{u}u \rangle_0) + m_s(\langle \bar{s}s \rangle - \langle \bar{s}s \rangle_0)]$ .

It is interesting to define the following quantity [45];

$$\chi_q^{(4)} = T \frac{\partial^4(-\Omega_{\text{PNJL}}/T)}{\partial \mu^4}, \quad (24)$$

and take the ratio to the quark number susceptibility. This ratio,  $\chi_q^{(4)}/\chi_q$ , counts the number squared of quark content inside thermally excited particles carrying baryon number. Therefore, if quarks are liberated in the high temperature region,  $\chi_q^{(4)}/\chi_q \simeq 1^2$  should follow, whereas the low temperature side should result in  $\chi_q^{(4)}/\chi_q \simeq 3^2$  because of confinement.

Figure 6 shows this susceptibility ratio obtained in the  $2 + 1$  flavor PNJL model. We see that the behavior perfectly fits what is expected. A short conclusion that we should learn from this analysis is that  $\chi_q^{(4)}/\chi_q$  signifies the quark number but does not tell us whether the thermally excited particle is a confined nucleon or a set of three quarks. The latter is the case in the PNJL model.

### E. More Thermodynamics

Before proceeding into the finite density inquiry, we shall exemplify the success of the PNJL model by two more thermodynamic quantities.

The trace of the energy momentum tensor is vanishing at the classical level when theory has no mass scale. We know that QCD in the chiral limit is scale invariant, which means that the trace of the energy momentum tensor in massless QCD is zero unless quantum corrections are taken into account. The QCD scale  $\Lambda_{\text{QCD}}$  arises from the dimensional transmutation due to the trace anomaly at the quantum level.

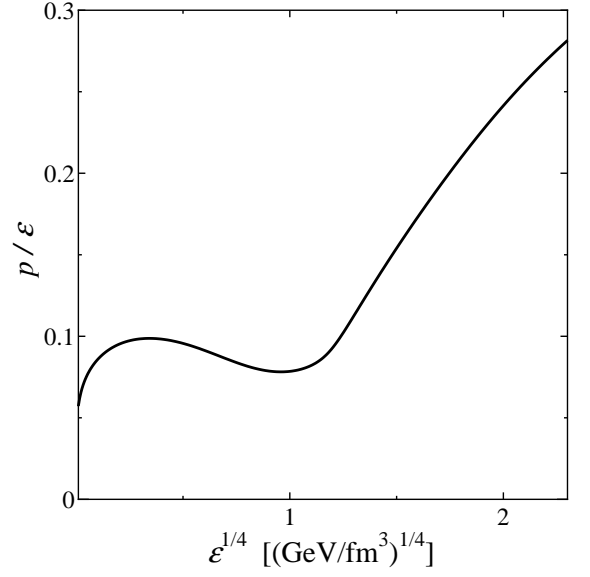


FIG. 8: Plot for  $p/\epsilon$  as a function of  $\epsilon^{1/4}$ .

In thermodynamics the traceless of the energy momentum tensor without mass gap means  $\epsilon - 3p = 0$  where  $p$  is the pressure given by  $-\Omega_{\text{PNJL}}$  and  $\epsilon$  is the internal energy given by  $T^2 \partial(p/T)/\partial T$ . It is straightforward to evaluate  $\epsilon - 3p$  or the “interaction measure” from  $\Omega_{\text{PNJL}}$  in our model study.

We show the model results in Fig. 7. The gross structure with a peak around  $T_c$  is in nice agreement with the recent lattice data (see Fig. 4 in Ref. [19]). The peak height in the interaction measure is not as large as that in Ref. [19], which is partly because of the finite number of  $N_\tau$  on the lattice and partly because of the smaller fermion contribution,  $\Theta_F^{\mu\mu}$ , in our calculation. We present the results for  $\Theta_F^{\mu\mu} = 2m_{ud}(\langle \bar{u}u \rangle - \langle \bar{u}u \rangle_0) + m_s(\langle \bar{s}s \rangle - \langle \bar{s}s \rangle_0)$  also in Fig. 7. We see that our results are significantly smaller than the results shown in Fig. 5 in Ref. [19]. This is because the quark mass is different; the  $\pi$  mass in Ref. [19] is still around 220 MeV, while we choose  $m_{ud}$  to yield the realistic  $\pi$  mass.

We should be aware that the interaction measure,  $(\epsilon - 3p)/T^4$ , has only little to do with the trace anomaly in the PNJL model study. We have model inputs with mass dimension, that is, the cutoff  $\Lambda$ . (There are four more dimensional parameters,  $g_S$ ,  $g_D$ ,  $a$ , and  $b$  but they can be all dimensionless in unit of  $\Lambda$ .)

As a matter of fact, the peak structure is rather generic regardless of any specific model. One can understand this from the thermodynamic relation,

$$\frac{\epsilon - 3p}{T^4} = T \frac{\partial}{\partial T} \left( \frac{p}{T} \cdot \frac{1}{T^3} \right). \quad (25)$$

The right-hand side is the temperature derivative of  $p/T^4$  where  $p/T^4$  naively counts the effective degrees of freedom  $\nu$  as plotted in Figs. 1 and 3. Therefore, so-called the trace anomaly,  $\epsilon - 3p$ , signifies how quickly  $\nu$  grows up as

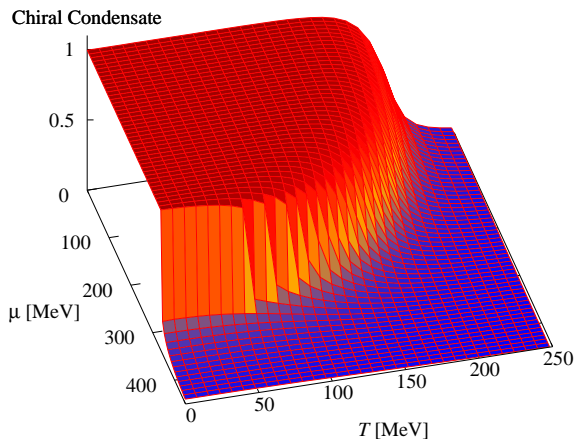


FIG. 9: Normalized light-quark chiral condensate  $\langle \bar{u}u \rangle / \langle \bar{u}u \rangle_0$  in the  $\mu$ - $T$  plane, where  $\langle \bar{u}u \rangle_0$  is the chiral condensate at  $T = \mu = 0$ .

$T$  increases. The pseudo-critical temperature is, by definition, where  $\nu$  starts getting larger, and eventually  $\nu$  is saturated to the total number of particle species at high temperature. As a result the peak shape is inevitable associated with crossover behavior. It is not quite surprising in this sense that the PNJL model can mimic the trace anomaly in hot QCD around  $T_c$ .

In other words, it is the relation between  $\epsilon - 3p$  and the gluon condensate that is a non-trivial consequence from the trace anomaly. The interaction measure,  $(\epsilon - 3p)/T^4$ , is governed not by the anomaly but by the thermodynamics which determines the gluon condensate in turn.

Now that we have come by the pressure and the internal energy, we can infer the sound velocity. Although the velocity of sound is given by  $c_s^2 = dp/d\epsilon$ , the ratio  $p/\epsilon$  can approximate it in the high temperature limit. To compare our results to the available lattice data, we plot  $p/\epsilon$  as a function of  $\epsilon^{1/4}$  in Fig. 8, which agrees quite well with Fig. 9 in Ref. [19]. We remark that the sound velocity has been investigated by means of the two-flavor PNJL model also in Ref. [46] where both of  $c_s^2$  and  $p/\epsilon$  are presented.

## V. FINITE DENSITY RESULTS

By adding one more axis in the direction of quark chemical potential we can investigate the order parameter behavior and the phase structure in wider perspective. In this work we limit ourselves to the chiral and deconfinement phase transitions and do not take account of the diquark condensation that plays an essential role in the color superconducting phase [39, 47, 48, 49].

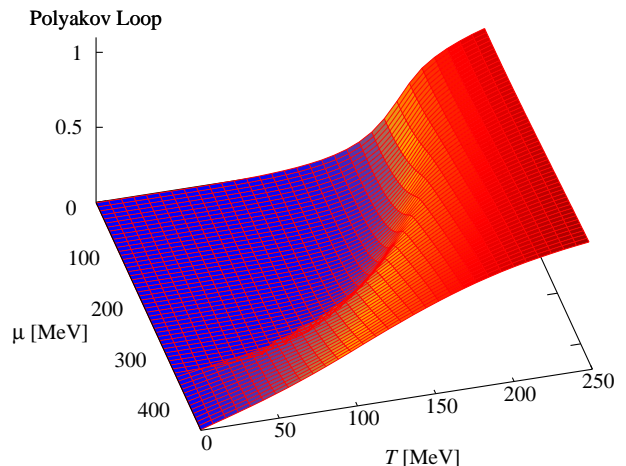


FIG. 10: Polyakov loop  $\ell$  in the  $\mu$ - $T$  plane.

### A. Chiral Phase Transition

Figure 9 is a 3D plot for  $\langle \bar{u}u \rangle$  as a function of  $T$  and  $\mu$ . We see that there is a discontinuity in the low temperature and high density region, while the high temperature and low density region has continuous crossover. Therefore the phase diagram has an end-point of the first-order phase boundary, that is called the QCD critical point. We remark that in the present parameter set the constituent quark masses turn out to be

$$M_{ud} = 336 \text{ MeV}, \quad M_s = 528 \text{ MeV}, \quad (26)$$

and the first-order phase transition is located at  $\mu = 345 \text{ MeV}$  when  $T = 0$ , which is slightly above the light quark mass. This is a general feature to be explained intuitively. First, let us focus on the region at  $\mu < 345 \text{ MeV}$  where the system does not have any discontinuous transition along the  $T = 0$  density axis. We can still locate the point where a nonvanishing baryon density appears at  $\mu = M_{ud}$ , that is a sort of continuous phase transition from the empty vacuum to degenerate quark matter. Next, once quark matter is concerned at  $\mu \simeq 345 \text{ MeV}$ , the pressure of cold quark matter at a fixed value of  $\mu$  becomes smaller for larger quark mass; for instance  $p \propto \mu^4$  for massless quarks and  $p \propto (\mu^2 - M^2)^2$  for massive quarks. Thus, the kinetic energy favors lighter quark matter, that is, the chiral symmetric phase. The condensation energy gives a negative contribution to the pressure, that means that the chiral symmetric phase where the condensation energy is smaller is energetically favorable again. In this way, one can expect that, as soon as the quark number density becomes substantial with  $\mu$  going above  $M_{ud}$ , the system tends to undergo a phase transition to the chiral symmetric phase.

## B. Polyakov Loop

It is interesting to see what happens in the Polyakov loop behavior on the  $\mu$ - $T$  plane. One may well anticipate that the coincidence of chiral restoration and deconfinement should persist in the finite density region. This expectation is partially true and partially untrue. We shall discuss the appropriate physical interpretation in what follows below.

We plot the Polyakov loop  $\ell$  in the  $\mu$ - $T$  plane in Fig. 10. It should be mentioned that we do not make another plot for  $\bar{\ell}$ , for  $\bar{\ell}$  has a qualitatively same functional shape as  $\ell$  with small quantitative difference.

From the comparison between the chiral condensate displayed in Fig. 9 and the Polyakov loop in Fig. 10, we can readily perceive that two crossovers are linked in the entire region on the  $\mu$ - $T$  plane. For instance, we have already confirmed that two crossovers are simultaneous indeed at zero density in Fig. 2, and we can find a first-order phase transition along the density axis at low temperature whose location is exactly the same in Figs. 9 and 10. The locking of chiral restoration and deconfinement remains at finite density in this sense.

It would be misleading, however, to dive into a conclusion that two phenomena of chiral restoration and deconfinement simultaneously take place in the high density region. In view of the Polyakov loop behavior at low temperatures, in fact, the discontinuous jump is tiny and the expectation value of the Polyakov loop stays vanishingly small even at  $\mu > 345$  MeV where chiral symmetry is restored. Therefore, the discontinuous jump in the Polyakov loop signifies a first-order phase transition from nearly confined matter ( $\ell \simeq 0$ ) with chiral symmetry breaking ( $\langle \bar{u}u \rangle \neq 0$ ) to nearly confined matter ( $\ell \simeq 0$ ) with chiral symmetry restoration ( $\langle \bar{u}u \rangle \simeq 0$ ).

It is an interesting question how the Polyakov loop behaves such differently from the chiral condensates in the region of low temperature and high density. This is because center symmetry is not broken at zero temperature even in the presence of dynamical quarks, and therefore, the expectation value of the Polyakov loop must stay vanishing. The reason for preserved center symmetry is to be understood intuitively as follows; when the quark density is specified by a certain chemical potential, each energy level is occupied by a quark up to the Fermi surface. Because quarks have color degeneracy, red, green, and blue quarks always sit on the same energy level, which makes a color singlet. One can easily see this really happening in the model from the Dirac determinant given in Eqs. (11) and (12). That is, when  $\mu > \varepsilon$  we only have the second term out of the whole particle contribution,

$$1 + e^{3|\varepsilon-\mu|/T} + 3\ell e^{|\varepsilon-\mu|/T} + 3\bar{\ell} e^{2|\varepsilon-\mu|/T}, \quad (27)$$

that is exponentially dominant for large  $|\varepsilon - \mu|/T$ . This second term,  $e^{3|\varepsilon-\mu|/T}$ , actually represents the three-quark occupation which does not couple  $\ell$  and thus not break center symmetry. The third and fourth terms are one-quark and two-quark (which is equivalent to one

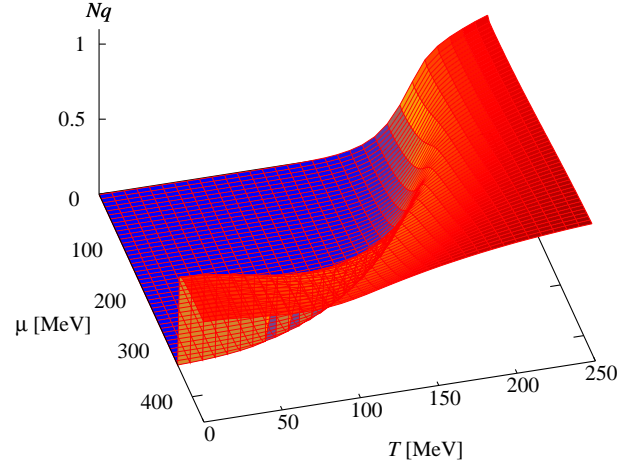


FIG. 11: Quark number density normalized by the free massless quark density,  $N_c N_f (\mu^3/3\pi^2 + T^2\mu/3)$ , in the  $\mu$ - $T$  plane.

anti-quark in color) contributions with non-trivial (non-singlet) color. Consequently, the Polyakov loop is insensitive to whether the quark degrees of freedom are present in the system or not. Strictly speaking, the PNJL model cannot deal with confinement, namely, nucleon wavefunctions as a bound state out of three quarks, but still, the low temperature region always has a signature of confinement ( $\ell \simeq 0$ ) with respect to quarks. We would stress that this quarky confined phase is not a model artifact but physical one. We propose that this phase should be identified as the *quarkyonic phase* discussed in Ref. [50].

One important suggestion emphasized in Ref. [50] is that the baryon or quark number density serves as an order parameter to tell the quarkyonic phase from the hadronic phase. We have then calculated the quark number density in the  $\mu$ - $T$  plane to make a plot of Fig. 11. The quark number density is readily available from

$$n_q = -\frac{\partial \Omega_{\text{PNJL}}}{\partial \mu}. \quad (28)$$

In order to visualize in a sensible manner on the 3D plot, we normalize  $n_q$  by the free massless quark density given by  $N_c N_f (\mu^3/3\pi^2 + T^2\mu/3)$ , that is, in Fig. 11 we plot,

$$N_q = \frac{n_q}{3\mu^3/\pi^2 + 3T^2\mu}, \quad (29)$$

which should take a value from zero to unity.

We can clearly confirm that the quark degrees of freedom are relevant (i.e.  $N_q \sim \mathcal{O}(1)$ ) even in the region at  $T \simeq 0$  and  $\mu > M_{ud}$  where  $\ell \simeq 0$ . This gives another evidence for our identification to the quarkyonic phase.

It is a non-trivial finding from the present PNJL model study that  $N_q$  surely behaves as an order parameter and locates the crossover point that coincides the chiral phase transition point. This coincidence is apparent at a glance of Figs. 9 and 11.

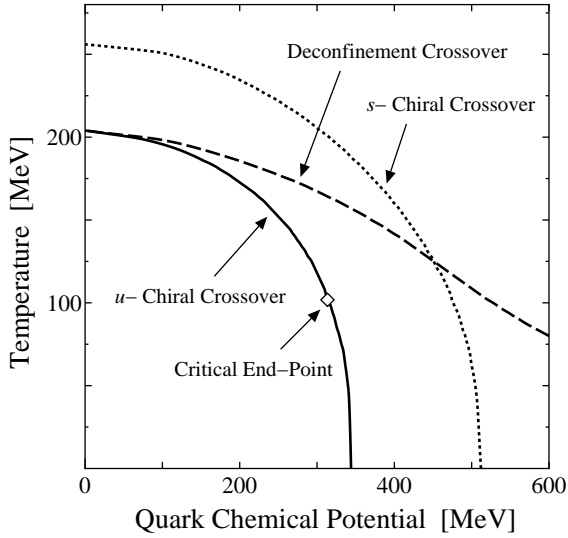


FIG. 12: Phase diagram characterized by three quantities, namely, the  $u$ -quark chiral condensate, the  $s$ -quark chiral condensate, and the Polyakov loop.

### C. Phase Diagram

We now explore the phase diagram in the  $\mu$ - $T$  plane by the cross-section of Figs. 9, 10, and 11 at a certain height in the vertical axis. As we discussed, in the high density region in particular, the susceptibility peak position does not make much sense, but the magnitude of the order parameter is a more suitable quantity to probe the physical state of matter. Therefore we define the pseudo-critical temperature for  $u$ -quark chiral restoration by the condition;

$$\left. \frac{\langle \bar{u}u \rangle}{\langle \bar{u}u \rangle_0} \right|_{T=T_u(\mu)} = \frac{1}{2}. \quad (30)$$

In the same way we can define the pseudo-critical temperature for  $s$ -quark chiral restoration by

$$\left. \frac{\langle \bar{s}s \rangle}{\langle \bar{s}s \rangle_0} \right|_{T=T_s(\mu)} = \frac{1}{2}. \quad (31)$$

Also, we can define the pseudo-critical temperature for deconfinement by

$$\left. \ell \right|_{T=T_\ell(\mu)} = \frac{1}{2}. \quad (32)$$

Then, we can draw three distinct curves by  $T = T_u(\mu)$ ,  $T_s(\mu)$ ,  $T_\ell(\mu)$  on the  $\mu$ - $T$  phase diagram. The PNJL model prediction is shown in Fig. 12. The solid curve represents  $T = T_u(\mu)$  which is crossover in the low density region and turns a first-order phase transition in the high density region accompanied by a critical end-point. We note that  $N_q$  is nearly zero inside this solid curve. Because of

explicit symmetry breaking by  $m_s \neq 0$ , the  $T = T_s(\mu)$  boundary is located at higher  $T$  and  $\mu$  shown by the dotted curve in Fig. 12. Of course, strictly speaking, chiral symmetry or even  $SU_V(3)$  symmetry is not restored at any temperature or density, but  $\langle \bar{s}s \rangle$  can decrease up to a half of  $\langle \bar{s}s \rangle_0$  smoothly. Actually this boundary hits  $T = 0$  and  $\mu = 512$  MeV which is not far from the constituent  $s$ -quark mass. In any case, the boundary by the dotted curve does not have a strong meaning because the change in  $\langle \bar{s}s \rangle$  as a function of  $T$  is only gradual. Nevertheless, the region bounded by  $T_u(\mu) < T < T_s(\mu)$  is interesting. This is because the  $SU_V(3)$  symmetry breaking becomes enhanced further in this region by chiral restoration for  $u$ -quarks and  $d$ -quarks but not for  $s$ -quarks [51].

It is surprising that the deconfinement crossover defined by the condition (32) goes away from the chiral phase transition at finite density as indicated by the dashed curve which represents the  $T = T_\ell(\mu)$  curve. As we have discussed, the Polyakov loop expectation value is always vanishing at zero temperature, and thus, this  $T = T_\ell(\mu)$  curve never hits the horizontal axis at  $T = 0$ . The region surrounded by  $T_u(\mu) < T < T_\ell(\mu)$  is what should be called the quarkyonic phase embodied in the PNJL model.

As a final remark in this section we refer to the similar results presented in Figs. 16 and 17 in Ref. [44] and the similar physical picture to the quarkyonic phase discussed in a different context in Ref. [52].

## VI. QCD CRITICAL END-POINT

We have already mentioned on the QCD critical end-point in the explanation of Fig. 12. The rest of this paper will be devoted to physics related to the QCD critical point. First of all, it is instructive to elucidate how the location of the critical point moves by the effect of the Polyakov loop. In the three-flavor NJL model with the Hatsuda-Kunihiro parameters, the location of the critical point is found to be

$$(T_E, \mu_E) = (48 \text{ MeV}, 324 \text{ MeV}), \quad (33)$$

in the three-flavor NJL model. The location is almost the same as in the two-flavor case. [See Ref. [54] for a summary table and also Ref. [53].] The model dependence is nicely compiled also on Fig. 4 in Ref. [55]. In the three-flavor PNJL model the location goes up along the temperature to

$$(T_E, \mu_E) = (102 \text{ MeV}, 313 \text{ MeV}), \quad (34)$$

in the present parameter set. This value is close to the two-flavor PNJL location first reported in my paper [13]. The reason why the critical point moves toward higher temperature and density is suppressed by the Polyakov loop average as exhibited in Fig. 3 and also discussed around Eq. (27).

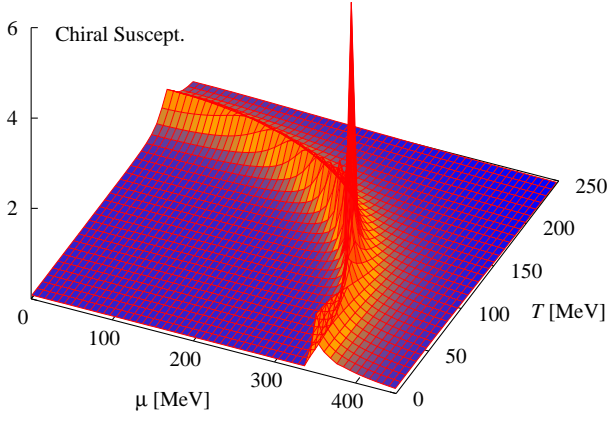


FIG. 13: 3D plot for the light-quark chiral susceptibility  $\chi_{ud}$  multiplied by  $(T/\Lambda)^2$  in the  $\mu$ - $T$  plane.

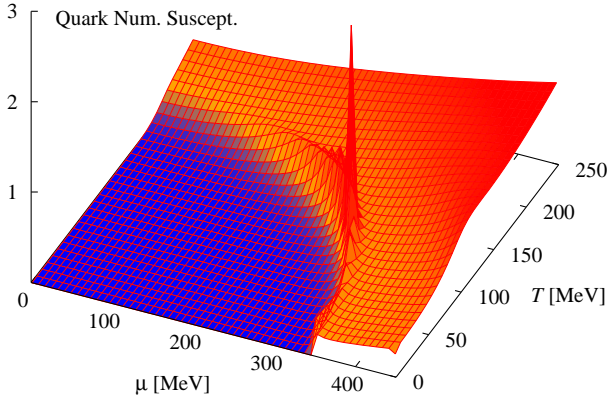


FIG. 14: 3D plot for the quark number susceptibility  $\chi_q$  multiplied by  $(T/\Lambda)^2$  in the  $\mu$ - $T$  plane.

The question is to what extent we can trust the model prediction for the location of the QCD critical point or even its existence. In what follows we will discuss the dependence on ambiguous model parameters. So far, it is quite difficult to make any robust statement about the QCD critical point from model studies, that is our short conclusion.

### A. Divergent Susceptibility

Before addressing the theoretical uncertainty on the QCD critical end-point, we will begin with standard arguments, that is, physical implication from the assumption that the QCD phase diagram holds a critical end-point.

The importance of the QCD critical point lies in the fact that it is an exact second-order phase transition point. Therefore the susceptibility diverges right at the end-point. Originally divergent growth in the chiral susceptibility  $\chi_u$  has been paid attention [56] which might lead to furious fluctuations in the  $\sigma$  channel and thus  $\pi$  fluctuations through the  $\sigma \leftrightarrow 2\pi$  cou-

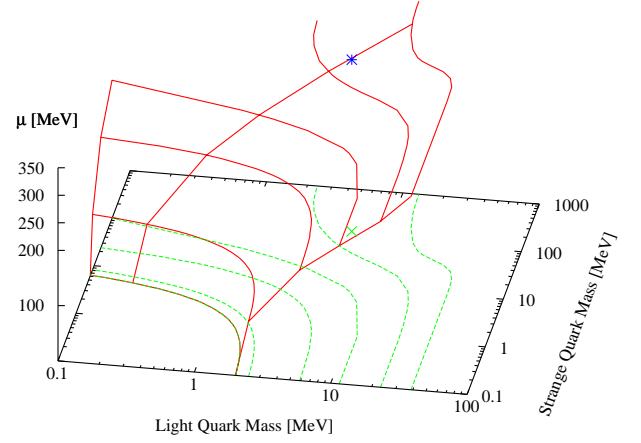


FIG. 15: Boundaries of the first-order phase transition region as a function of the quark masses at  $\mu = 0, 100, 200, 250, 300, 350$  MeV from the bottom to the top.

pling. We have made a 3D plot in Fig. 13 to show the  $u$ -quark chiral susceptibility multiplied by  $(T/\Lambda)^2$ , i.e.  $-\frac{1}{4}\Lambda^{-2}\partial^2\Omega_{\text{PNJL}}/\partial m_{ud}^2$  in the  $\mu$ - $T$  plane. We notice that the susceptibility has a singularity at the critical point.

A physical quantity of more experimental interest is the quark number susceptibility. We plot  $\chi_q$  multiplied by  $(T/\Lambda)^2$  in Fig. 14, that is,  $-\Lambda^{-2}\partial^2\Omega_{\text{PNJL}}/\partial \mu^2$  in the  $\mu$ - $T$  plane. Figure 14 shows a singularity at the QCD critical point which should translate into event-by-event fluctuations of baryon multiplicity. The global shape is just similar to that of the chiral susceptibility. It is, however, different that the quark number susceptibility gets non-vanishing in the high temperature or density region whose behavior is closely linked to the quark number density in Fig. 11.

### B. Columbia Diagram

What we will reveal particularly in this work is the robustness of the existence of the critical end-point, which is in part motivated by the lattice suggestion [57]. We can disclose another aspect of the phase diagram in the plane of the light and heavy quark masses [58]. Such a phase diagram is sometimes referred to as the “Columbia Diagram.”

The PNJL model results are summarized in Fig. 15. Each curve represents the boundary between the first-order phase transition to the crossover. For  $m_{ud}$  and  $m_s$  below the curve, the chiral phase transition at finite  $T$  is of first-order, and otherwise, it is crossover. We draw a line  $m_s/m_{ud} = 24.67$  which crosses the physical point, and add two lines at  $m_{ud} = 0$  and  $m_s = 0$ , respectively, for the eye guide.

This plot poses us a problem in the model study based on the NJL-type description. It is that the first-order phase transition region at  $\mu = 0$  is substantially smaller than what has been observed in the lattice QCD simu-

lations. In the  $m_s = 0$  case, for instance, the critical value of the light-quark mass is  $m_u = 2.1$  MeV in this work, and on the  $m_{ud} = 0$  axis, the critical strange quark mass is  $m_s = 8.8$  MeV, which are smaller by one order of magnitude at least as compared to the lattice empirical value [57]. This fact implies that the first-order phase transition with massless three flavors is presumably weaker in the NJL model than realistic. Then, the critical end-point at physical quark mass cannot avoid being far away from zero density. That is, the density has to increase significantly until the boundary eventually hits the physical mass point. This is why the NJL-type model has common tendency to lead to the critical end-point at relatively high density above  $\mu \sim 300$  MeV.

Because the PNJL model predicts the QCD critical point, the first-order transition region expands with increasing  $\mu$  as shown in Fig. 15. The boundary surface is thus standard but not quite consistent with the recent lattice observation [57]. This is problematic to the model study if the lattice results are correct. The model study has, however, unknown factors which could make a drastic change in the order. Here, we will point out two major effects; one is the  $U_A(1)$  anomaly reduction in a medium and the other is the induced vector-channel interaction.

### 1. Anomaly strength

We have already noted that the first-order transition region on the Columbia diagram obtained in the PNJL model is significantly smaller than the lattice results. One likely explanation for this is that the 't Hooft (six-quark) coupling constant,  $g_D$ , is weaker in the NJL model estimate than realistic because of cutoff artifact. It should be mentioned that the value of  $g_D$  is fixed to reproduce the  $\eta'$  mass, which is as large as 957.5 MeV and is greater than the cutoff  $\Lambda = 631.4$  MeV. It is not unlikely that the strength of  $g_D$  has been underestimated to reproduce such a large mass in this cutoff model.

Figure 16 shows the first-order transition boundary on the  $m_{ud}$ - $m_s$  plane. Here  $g_{D0}$  denotes the standard value in the Hatsuda-Kunihiro parameter set. Because  $g_{D0}$  has been fixed in the vacuum,  $g_D$  in a hot and dense medium might take a different (presumably smaller) value. As we anticipated, the first-order region becomes wider with larger  $g_D$  and narrower with smaller  $g_D$ . It should be noted that the plot is made in the linear scale in Fig. 16, while the scale is logarithmic in Fig. 15.

One can then expect that the QCD critical point should move accordingly as  $g_D$  changes. We show the location of the QCD critical point for various values of  $g_D$  in Fig. 17. We can learn two lessons from this figure: One is that the QCD critical point can be located at higher temperature and lower density if  $g_D$  is underestimated in the NJL model study due to too heavy  $\eta'$  out of model reliability. The other is in a sense opposite to the first one. The QCD critical point might be absent from the QCD phase diagram if  $g_D$  is suppressed

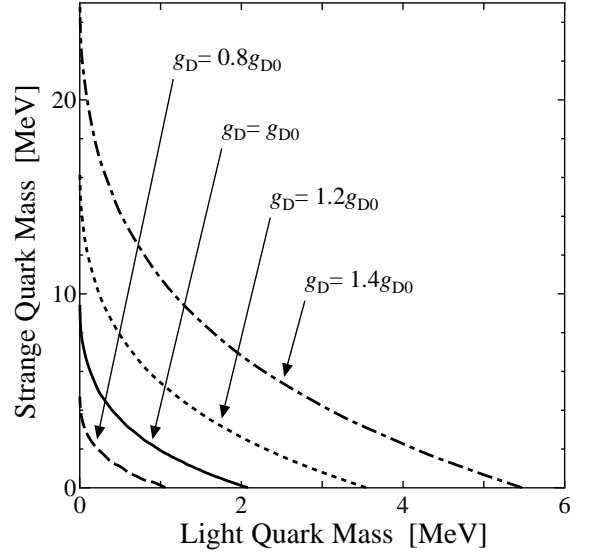


FIG. 16: First-order transition boundary depending on the strength of the 't Hooft coupling  $g_D$ , where  $g_{D0}$  is a value fixed in the vacuum in the Hatsuda-Kunihiro parameter set.

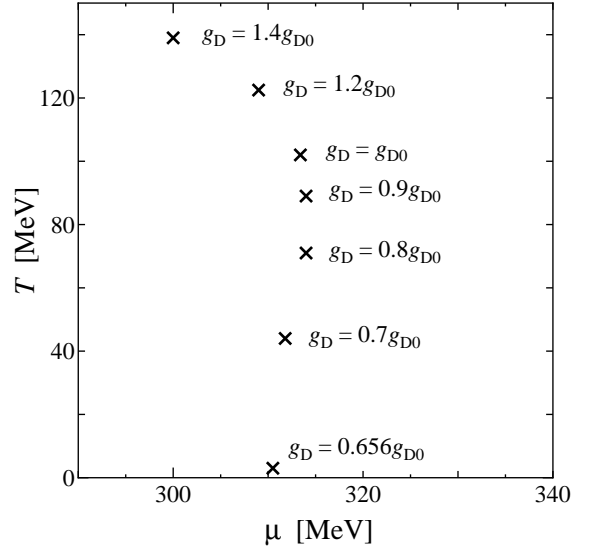


FIG. 17: Dependence of the critical point location on the strength of the 't Hooft coupling constant.

by the effective  $U_A(1)$  restoration at high density. Actually, only 35% reduction is enough to make the QCD critical point disappear from the phase diagram. If the suppression is exponential like  $g_D(\mu) = e^{-\mu^2/\mu_0^2} g_{D0}$  [12], 35% reduction is within a reasonable reach.

Then, one could change the scenario in Fig. 15 by introducing a  $\mu$ -dependent value for  $g_D$ . For instance, if one assumes an exponential ansatz,  $g_D(\mu) = e^{-\mu^2/\mu_0^2} g_{D0}$ , one could find some  $\mu_0$  that produces a boundary surface with bending behavior that the first-order transition region shrinks with increasing  $\mu$ .



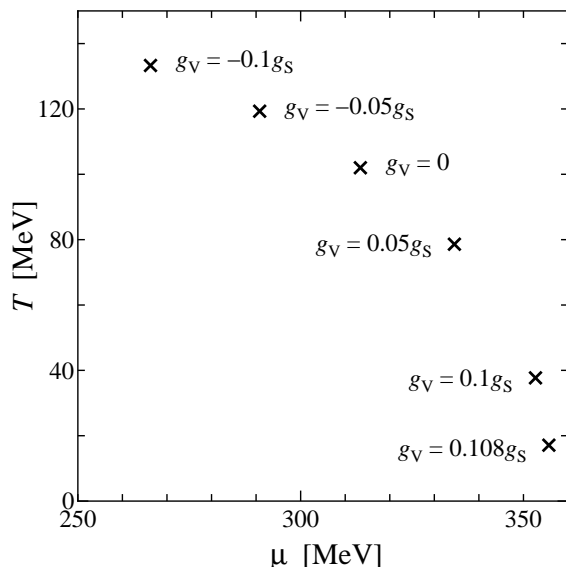


FIG. 18: Dependence of the critical point location on the strength of the vector-channel interaction.

## 2. Vector-channel interaction

It is not only the  $U_A(1)$  anomaly term but also the vector-channel interaction term in Eq. (4) that can affect the location of the QCD critical point. We remark that  $\mathcal{L}_V$  does not break chiral symmetry at all, and besides, the zeroth component corresponds to the density operator  $(\psi^\dagger\psi)^2$ . Therefore, it is conceivable to expect that the finite density environment brings about non-zero  $g_V$  even though we choose  $g_V$  to be zero in the vacuum.

There is no constraint at all for the choice of induced  $g_V$  at finite density. We have no knowledge on even its sign. Since we regard  $g_V$  in the present study as induced in dense quark matter, the choice of  $g_V$  has nothing to do with the vector meson property in the vacuum. [It might be related to an in-medium modification.] It is presumably appropriate to measure the strength of  $g_V$  in unit of  $g_S$ , and we just try various values of  $g_V$  to grasp a feeling of its effect.

There are two modifications necessary to accommodate the vector-channel interaction. The condensation energy should be  $\Omega_{\text{cond}} \rightarrow \Omega_{\text{cond}} - g_V n_q^2$  where we already defined  $n_q$  in Eq. (28). At the same time, the quark chemical potential should be replaced by the renormalized one,

$$\mu_r = \mu - 2g_V n_q, \quad (35)$$

like the quark mass replaced by the constituent one. Then, we have to solve the number constraint equation,  $n_q = -\partial\Omega_{\text{PNJL}}/\partial\mu_r$ , together with the four gap equations self-consistently. In view of the condensation energy part, positive  $g_V$  seems to decrease the free energy for non-zero  $n_q$ , but the chemical potential renormalization overcomes it and the free energy becomes greater. Because chiral symmetric phase has smaller  $M_{ud}$  and thus

larger  $n_q$ , the vector-channel interaction with  $g_V > 0$  delays chiral restoration.

The results are summarized in Fig. 18 in the same way as in Fig. 17. It is remarkable that the qualitative feature is quite similar to Fig. 17. Thus, we can draw the same conclusions as in the case of the  $U_A(1)$  anomaly term.

The QCD critical point could be absent again in the case when  $g_V$  is greater than around  $0.108g_S$ . The critical value turns out to be much smaller than the known value [32]. This discrepancy stems from the difference between the two-flavor and three-flavor calculations; we calculated the critical  $g_V$  in the standard NJL model with three flavors and found it to be almost the same  $\sim 0.11g_S$ . That also means that the Polyakov loop plays a minor role. In the three-flavor treatment in comparison to the two-flavor case  $n_q$  becomes larger generally and  $g_S$  is different as well.

Nevertheless, this value of critical  $g_V$  seems to be surprisingly small. If we take care of the effect of the effective  $U_A(1)$  restoration, as we illustrate in Fig. 17, the critical  $g_V$  could be even smaller.

## VII. CONCLUSIONS

We have formulated the 2 + 1 flavor PNJL model with a simple ansatz for the Polyakov loop effective potential. We first confirmed that our model setup works pretty well to account for recent results in the zero-density lattice QCD simulation. We then explored our perspective toward the finite-density QCD phase transition.

The phase diagram in our model study turns out to have three (crossover) boundaries corresponding to  $ud$ -quark chiral restoration,  $s$ -quark chiral restoration, and deconfinement characterized by the Polyakov loop expectation value. We have also computed the quark number density and found that its behavior is governed by the  $u$ -quark chiral condensate. Our phase diagram is consistent with the large  $N_c$  argument and, in particular, we identified the phase region with vanishing Polyakov loop and nonzero quark number density as the quarkyonic phase.

It would be intriguing to include the diquark condensates to describe a family of the color superconducting phases. The large  $N_c$  argument cannot access physics of color superconductivity, and thus, nothing so far could predict the fate of the quarkyonic phase region under the effect of color superconductivity. One possibility is that the quark-hadron continuity realizes at low temperature and high density, and there appears crossover from the quarkyonic phase to the color superconducting phase, which is to be interpreted as crossover from confined to deconfined quark matter.

Also, we have closely investigated parameter dependence of the location of the QCD critical point. We demonstrated that the QCD critical point moves quite easily in accord to the choice of the  $U_A(1)$  anomaly strength and the vector-channel interaction. Both are not under theoretical control at finite density. In fact,

we have found that the critical values of these parameters are within a conceivable range in dense quark matter. That means, not only the location but also the existence of the QCD critical point is not robust at all in the model study.

Although we limited our discussions only to numerical results in this paper, it could be viable to examine the density dependence of the Columbia diagram in an analytical way [59]. Analytical understanding should be useful for the lattice QCD study from the zero density approaching toward the critical point.

To establish the existence or non-existence of the QCD critical point, anyway, we must wait for future develop-

ment of the finite-density lattice simulation, or experimental confirmation. [See also Refs. [60, 61] for proposed experimental signatures.]

### Acknowledgments

The author thanks Ph. de Forcrand, T. Kunihiro, L. McLerran, R. Redlich, C. Sasaki, M. A. Stephanov, and W. Weise for discussions. This work is in part supported by Yukawa International Program for Quark-Hadron Sciences.

- 
- [1] For earliest works, see; N. Itoh, Prog. Theor. Phys. **44**, 291 (1970); J. C. Collins and M. J. Perry, Phys. Rev. Lett. **34**, 1353 (1975).
  - [2] For reviews, see; B. Svetitsky, Phys. Rept. **132**, 1 (1986); H. Meyer-Ortmanns, Rev. Mod. Phys. **68**, 473 (1996) [arXiv:hep-lat/9608098]; D. H. Rischke, Prog. Part. Nucl. Phys. **52**, 197 (2004) [arXiv:nucl-th/0305030].
  - [3] J. B. Kogut, M. Stone, H. W. Wyld, W. R. Gibbs, J. Shigemitsu, S. H. Shenker and D. K. Sinclair, Phys. Rev. Lett. **50**, 393 (1983).
  - [4] G. Baym, Nucl. Phys. A **698**, XXIII (2002) [arXiv:hep-ph/0104138].
  - [5] M. Fukugita and A. Ukawa, Phys. Rev. Lett. **57**, 503 (1986).
  - [6] Y. Aoki, Z. Fodor, S. D. Katz and K. K. Szabo, Phys. Lett. B **643**, 46 (2006) [arXiv:hep-lat/0609068].
  - [7] A. Gocksch and M. Ogilvie, Phys. Rev. D **31**, 877 (1985).
  - [8] E. M. Ilgenfritz and J. Kripfganz, Z. Phys. C **29**, 79 (1985).
  - [9] S. Digal, E. Laermann and H. Satz, Eur. Phys. J. C **18**, 583 (2001) [arXiv:hep-ph/0007175]; A. Mocsy, F. San- nino and K. Tuominen, Phys. Rev. Lett. **92**, 182302 (2004) [arXiv:hep-ph/0308135].
  - [10] Y. Hatta and K. Fukushima, Phys. Rev. D **69**, 097502 (2004) [arXiv:hep-ph/0307068]; arXiv:hep-ph/0311267.
  - [11] S. P. Klevansky, Rev. Mod. Phys. **64**, 649 (1992).
  - [12] T. Hatsuda and T. Kunihiro, Phys. Rept. **247**, 221 (1994) [arXiv:hep-ph/9401310].
  - [13] K. Fukushima, Phys. Lett. B **591**, 277 (2004) [arXiv:hep-ph/0310121].
  - [14] K. Fukushima, Phys. Lett. B **553**, 38 (2003) [arXiv:hep-ph/0209311]; Phys. Rev. D **68**, 045004 (2003) [arXiv:hep-ph/0303225]; Prog. Theor. Phys. Suppl. **153**, 204 (2004) [arXiv:hep-ph/0312057].
  - [15] C. Ratti, M. A. Thaler and W. Weise, Phys. Rev. D **73**, 014019 (2006) [arXiv:hep-ph/0506234].
  - [16] W. j. Fu, Z. Zhang and Y. x. Liu, Phys. Rev. D **77**, 014006 (2008) [arXiv:0711.0154 [hep-ph]].
  - [17] M. Ciminale, R. Gatto, N. D. Ippolito, G. Nardulli and M. Ruggieri, arXiv:0711.3397 [hep-ph].
  - [18] K. Fukushima and Y. Hidaka, Phys. Rev. D **75**, 036002 (2007) [arXiv:hep-ph/0610323].
  - [19] M. Cheng *et al.*, Phys. Rev. D **77**, 014511 (2008) [arXiv:0710.0354 [hep-lat]].
  - [20] M. Asakawa and K. Yazaki, Nucl. Phys. A **504**, 668 (1989).
  - [21] A. Barducci, R. Casalbuoni, S. De Curtis, R. Gatto and G. Pettini, Phys. Lett. B **231**, 463 (1989); A. Barducci, R. Casalbuoni, G. Pettini and R. Gatto, Phys. Rev. D **49**, 426 (1994).
  - [22] J. Berges and K. Rajagopal, Nucl. Phys. B **538**, 215 (1999) [arXiv:hep-ph/9804233].
  - [23] M. A. Halasz, A. D. Jackson, R. E. Shrock, M. A. Stephanov and J. J. M. Verbaarschot, Phys. Rev. D **58**, 096007 (1998) [arXiv:hep-ph/9804290].
  - [24] Y. Hatta and T. Ikeda, Phys. Rev. D **67**, 014028 (2003) [arXiv:hep-ph/0210284].
  - [25] Z. Fodor and S. D. Katz, JHEP **0203**, 014 (2002) [arXiv:hep-lat/0106002].
  - [26] R. V. Gavai and S. Gupta, Phys. Rev. D **71**, 114014 (2005) [arXiv:hep-lat/0412035].
  - [27] R. D. Pisarski and F. Wilczek, Phys. Rev. D **29**, 338 (1984).
  - [28] E. V. Shuryak, Comments Nucl. Part. Phys. **21**, 235 (1994) [arXiv:hep-ph/9310253].
  - [29] T. D. Cohen, Phys. Rev. D **54**, 1867 (1996) [arXiv:hep-ph/9601216].
  - [30] K. Fukushima, K. Ohnishi and K. Ohta, Phys. Rev. C **63**, 045203 (2001) [arXiv:nucl-th/0101062].
  - [31] S. Klimt, M. Lutz and W. Weise, Phys. Lett. B **249**, 386 (1990).
  - [32] M. Kitazawa, T. Koide, T. Kunihiro and Y. Nemoto, Prog. Theor. Phys. **108**, 929 (2002) [arXiv:hep-ph/0207255].
  - [33] C. Sasaki, B. Friman and K. Redlich, Phys. Rev. D **75**, 054026 (2007) [arXiv:hep-ph/0611143].
  - [34] S. Chandrasekharan and S. z. Huang, Phys. Rev. D **53**, 5100 (1996) [arXiv:hep-ph/9512323].
  - [35] P. N. Meisinger and M. C. Ogilvie, Phys. Lett. B **379**, 163 (1996) [arXiv:hep-lat/9512011].
  - [36] C. R. Allton *et al.*, Phys. Rev. D **66**, 074507 (2002) [arXiv:hep-lat/0204010].
  - [37] A. Dumitru, R. D. Pisarski and D. Zschesche, Phys. Rev. D **72**, 065008 (2005) [arXiv:hep-ph/0505256].
  - [38] E. Megias, E. Ruiz Arriola and L. L. Salcedo, Phys. Rev. D **74**, 065005 (2006) [arXiv:hep-ph/0412308].
  - [39] S. Roessner, C. Ratti and W. Weise, Phys. Rev. D **75**, 034007 (2007) [arXiv:hep-ph/0609281].
  - [40] C. Ratti, S. Roessner and W. Weise, Phys. Lett. B **649**, 57 (2007) [arXiv:hep-ph/0701091].



- [41] K. Fukushima, *Annals Phys.* **304**, 72 (2003) [arXiv:hep-ph/0204302].
- [42] K. Fukushima, work in progress.
- [43] T. Kunihiro, *Phys. Lett. B* **271**, 395 (1991).
- [44] C. Sasaki, B. Friman and K. Redlich, *Phys. Rev. D* **75**, 074013 (2007) [arXiv:hep-ph/0611147].
- [45] S. Ejiri, F. Karsch and K. Redlich, *Phys. Lett. B* **633**, 275 (2006) [arXiv:hep-ph/0509051].
- [46] S. K. Ghosh, T. K. Mukherjee, M. G. Mustafa and R. Ray, *Phys. Rev. D* **73**, 114007 (2006) [arXiv:hep-ph/0603050].
- [47] M. Ciminale, G. Nardulli, M. Ruggieri and R. Gatto, *Phys. Lett. B* **657**, 64 (2007) [arXiv:0706.4215 [hep-ph]].
- [48] H. Abuki, M. Ciminale, R. Gatto, G. Nardulli and M. Ruggieri, arXiv:0802.2396 [hep-ph].
- [49] K. Fukushima, T. Kunihiro, Z. Zhang, work in progress.
- [50] L. McLerran and R. D. Pisarski, *Nucl. Phys. A* **796**, 83 (2007) [arXiv:0706.2191 [hep-ph]].
- [51] T. Kunihiro, in private communications.
- [52] L. Y. Glozman and R. F. Wagenbrunn, *Phys. Rev. D* **77**, 054027 (2008) [arXiv:0709.3080 [hep-ph]]; L. Y. Glozman, arXiv:0803.1636 [hep-ph].
- [53] P. Costa, C. A. de Sousa, M. C. Ruivo and H. Hansen, arXiv:0801.3616 [hep-ph].
- [54] K. Kashiwa, H. Kouno, M. Matsuzaki and M. Yahiro, arXiv:0710.2180 [hep-ph].
- [55] M. A. Stephanov, *PoS LAT2006*, 024 (2006) [arXiv:hep-lat/0701002].
- [56] M. A. Stephanov, K. Rajagopal and E. V. Shuryak, *Phys. Rev. Lett.* **81**, 4816 (1998) [arXiv:hep-ph/9806219]; *Phys. Rev. D* **60**, 114028 (1999) [arXiv:hep-ph/9903292].
- [57] P. de Forcrand and O. Philipsen, *JHEP* **0701**, 077 (2007) [arXiv:hep-lat/0607017]; P. de Forcrand, S. Kim and O. Philipsen, *PoS LAT2007*, 178 (2007) [arXiv:0711.0262 [hep-lat]].
- [58] F. R. Brown *et al.*, *Phys. Rev. Lett.* **65**, 2491 (1990).
- [59] M. A. Stephanov, in private communications.
- [60] Y. Hatta and M. A. Stephanov, *Phys. Rev. Lett.* **91**, 102003 (2003) [Erratum-ibid. **91**, 129901 (2003)] [arXiv:hep-ph/0302002].
- [61] M. Asakawa, S. A. Bass, B. Muller and C. Nonaka, arXiv:0803.2449 [nucl-th].